Journal of Magnetism and Magnetic Materials 353 (2014) 110–115

Contents lists available at ScienceDirect

Journal of Magnetism and Magnetic Materials

journal homepage: www.elsevier.com/locate/jmmm

Non-regularized inversion method from light scattering applied to ferrofluid magnetization curves for magnetic size distribution analysis

Jos van Rijssel [1], Bonny W.M. Kuipers [1], Ben H. Erné *

Van 't Hoff Laboratory for Physical and Colloid Chemistry, Debye Institute for Nanomaterials Science, Utrecht University, Padualaan 8, 3584 CH Utrecht, The Netherlands

ARTICLE INFO

Article history:
Received 28 March 2013
Received in revised form
2 October 2013
Available online 30 October 2013

Keywords:
AGM
VSM
Non-negative least squares fitting
Numerical method
DLS
SLS

ABSTRACT

A numerical inversion method known from the analysis of light scattering by colloidal dispersions is now applied to magnetization curves of ferrofluids. The distribution of magnetic particle sizes or dipole moments is determined without assuming that the distribution is unimodal or of a particular shape. The inversion method enforces positive number densities via a non-negative least squares procedure. It is tested successfully on experimental and simulated data for ferrofluid samples with known multimodal size distributions. The created computer program MINORIM is made available on the web.

1. Introduction

Magnetic nanoparticles have many applications that are the subject of current research. For example, in cancer therapy local hyperthermia can be generated by heating magnetic nanoparticles linked to cancer cells by applying an alternating magnetic field [1,2]. Another promising biomedical technique is magnetic particle imaging (MPI) [3], which also exploits the response of magnetic nanoparticles to alternating fields. Both of these biomedical applications ideally require magnetic particles that all have exactly the same (size dependent) magnetic resonance frequency [4,5], to obtain a maximum response at that frequency. For these and other applications, it is important to know how the magnetic properties are distributed across the entire population of nanoparticles. A widely adopted approach to determine the distribution of the dipole moments is by analysis of the magnetization of the sample as a function of external magnetic field strength.

The magnetization curves of ferrofluids are often fitted on the basis of an assumed shape of the distribution of the magnetic dipole moments, related more or less directly to the size distribution from transmission electron microscopy (TEM). Chantrell et al. [6] assumed a log-normal distribution, but other distributions such as a gamma function have been adopted as well [7,8]. The parameters of the log-normal distribution can either be derived from the low- and high-field limits of the magnetization curve [6,7] or from fitting the complete curve [9,10]. More specific models have also been proposed, like a core–shell model [11] to explain the discrepancy between magnetic diameter and physical diameter from TEM. For multimodal systems, the distribution can in principle be modeled with multiple peaks; one then faces the difficulty that an increasing number of fit parameters can make the results less reliable and physically less meaningful.

For dynamic light scattering as a colloidal characterization technique (DLS), there is a long tradition of obtaining particle size distributions without assuming the distribution shape but by applying discrete inversion methods [12]. Similar methods have also been used to derive magnetic particle size or dipole moment distributions from magnetization measurements [13–17]. An analysis technique that does not assume any shape of the particle distribution generally yields a better fit of the experimental magnetization curve.

Nowadays, many different inversion methods are available, such as genetic algorithms [13], maximum entropy [18], singular value decomposition (SVD) [19], simulated annealing [13], moment expansion [20], and non-negative least squares methods. The latter can be subdivided into a class of regularized methods, such as the CONTIN method [12,21,22], prominent in dynamic light scattering [12], and non-regularized methods [23]. The reconstruction of the magnetic size distribution by these techniques is not trivial and not necessarily robust. For example, the SVD method is highly sensitive to noise [6].

* Corresponding author. Tel.: +31 302532934.
E-mail address: B.H.Erne@uu.nl (B.H. Erné).
[1] Both authors contributed equally to this work.

0304-8853/$ - see front matter © 2013 Elsevier B.V. All rights reserved.
http://dx.doi.org/10.1016/j.jmmm.2013.10.025

For a good reconstruction based on the moments of the distribution, typically 10 moments are necessary to arrive at a reasonable approximation of the dipole moment distribution. Although these moments could be obtained via a fit of the magnetization curve with a Taylor expansion of the Langevin function, the number of terms required to describe a reasonable part of the data is large and therefore the reliability of the thus obtained moments is low. And although genetic algorithms can provide reliable distributions, these methods typically have a high computational cost.

In this paper, we apply a model-independent, non-regularized inversion method for the analysis of magnetization curves. It is adapted from a method designed by Strawbridge and Hallett [23] for the analysis of static light scattering measurements (SLS). This method does not assume unimodality nor other prior knowledge of the shape of the distribution of particle sizes or magnetic dipole moments. Using non-negative least squares procedures (NNLS), our method enforces positive number densities, unlike other methods that can give negative, unphysical results [15]. Our procedure is applicable to measurement data from alternating gradient magnetometry (AGM) as well as vibrating sample magnetometry (VSM).

In principle, our program is based on discrete sampling methods, originally developed by Pike et al. [24] as an exponential sampling technique, and later improved by Morrison et al. [25]. With the NNLS procedure based on Lawson and Hanson [26], a short execution time is obtained on the order of seconds or less using a state-of-the-art personal computer.

In the next section, the mathematical foundation of our model-independent method is presented. In the Results and Discussion section, the method is first demonstrated on real measurement data of ferrofluid samples with a known multimodal size distribution. This is followed by the analysis of simulated magnetization curves calculated for test distributions of the dipole moment. Gaussian noise is added to the simulated measurements to test the robustness of the inversion method.

2. Numerical methods

For a dilute dispersion of monodisperse non-interacting spherical magnetic nanoparticle dipoles, the total magnetic dipole moment M of the sample as a function of the applied magnetic field H is described by the Langevin function L, with

$$M(H) = M_{sat} L(H,\mu) = M_{sat}\left(\coth(\alpha) - \frac{1}{\alpha}\right) \quad \alpha = \left(\frac{\mu\mu_0 H}{k_B T}\right) \tag{1}$$

where M_{sat} is the magnetic moment of the sample under magnetic saturation conditions, μ is the magnetic dipole moment of a magnetic nanoparticle, μ_0 is the permeability of vacuum, k_B is the Boltzmann constant, and T is the absolute temperature. In case of a monodisperse ferrofluid with a number n of particles, M_{sat} corresponds to the magnetic moment $M_{sat} = n\mu$ when all magnetic dipoles are aligned in the limit of infinite applied field H. For a polydisperse or a multimodal colloidal dispersion, the sample magnetic moment is the sum of all contributing dipole moments, which for a continuous joint probability distribution function can be written as a distribution integral:

$$M(H) = \int_0^\infty \mu L(H,\mu) P(\mu)\, \mathrm{d}\mu \tag{2}$$

Here, the factor $P(\mu)\,\mathrm{d}\mu$ gives the number of particles with dipole moments between μ and $\mu+\mathrm{d}\mu$ and, similarly, $\mu P(\mu)\,\mathrm{d}\mu$ gives the contribution to the magnetic moment of the sample under saturation conditions.

In order to obtain the magnetic dipole moment distribution $P(\mu)$, we must solve Eq. (2) given the experimental magnetization curve $M_{\mathrm{exp}H}$ and using the Langevin function $L(H,\mu)$ from Eq. (1).

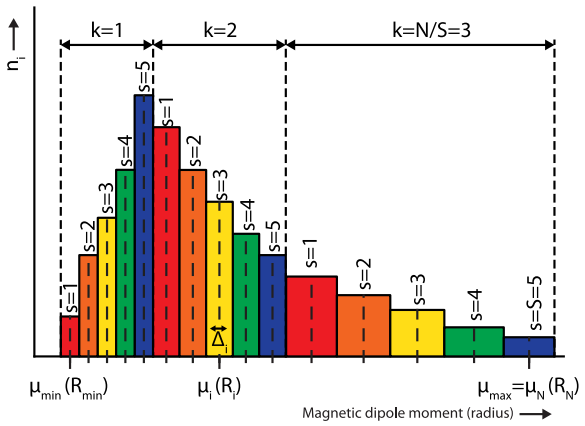

Fig. 1. Histogram showing an example of a dipole moment distribution with the dipole moments μ (or alternatively the particle radius R) binned in $N=15$ geometrically spaced bins, subdivided into $S=5$ subdomains. The meaning of the y-axis values depends on the definition of the probability factor $P(\mu)$ in the magnetization function (Eq. (2)).

This is in general an ill-conditioned problem; small experimental uncertainties such as noise can give rise to large, unphysical peaks in the distribution curve [12].

To address this problem, we rewrite Eq. (2) in a discrete form. The magnetic dipole moment domain is subdivided into a histogram of N intervals of which each bin spacing Δ_i has a center dipole moment μ_i and a bin content equal to the number amplitude n_i (see Fig. 1). The experimental magnetization curve consists of J points M_j each measured at a field strength H_j. The discrete form of Eq. (2) becomes

$$M_{exp}(H_j) = \sum_{i=1}^{N} \mu_i L(H_j,\mu_i) n_i \tag{3}$$

The basis vector $\mathbf{H}_j$ contains the experimental values of the magnetic field strength at which the measurements are made. The measurement output can be written as a column vector $\mathbf{M}_{exp}$ having the same length J. We describe the magnetic dipole moment distribution by a column vector $\mathbf{n}_{psd}$ of length N, with elements n_i in a basis μ_i. Eq. (3) can now be summarized using a $J\times N$ data transfer matrix $\overleftrightarrow{\mathbf{T}}$ that contains matrix elements T_{ji} equal to $\mu_i L(H_j,\mu_i)$ calculated using the Langevin function (see Eq. (1)):

$$\mathbf{M}_{exp} = \overleftrightarrow{\mathbf{T}} \cdot \mathbf{n}_{psd} \tag{4}$$

In the absence of experimental uncertainties, the number distribution $\mathbf{n}_{psd}$ can be solved from Eq. (4). Due to noise and other measurement uncertainties, statistical methods are needed to obtain the best magnetic dipole moment distribution n_i by minimizing the mean squares deviation ξ^2:

$$\xi^2 = \|[\mathbf{M}_{exp} - \overleftrightarrow{\mathbf{T}} \cdot \mathbf{n}_{psd}]\|^2 \tag{5}$$

The result of this inversion method is obtained without assuming prior knowledge of the form of the distribution (e.g., *log-normal* or *Gaussian*).

Regularization methods are often used in order to make the problem less ill-conditioned. In dynamic light scattering, the CONTIN method [12,21,22], based on the algorithm of Tikhonov [27,28], is a well-known example. A mathematical regularizing term is added to Eq. (5) to force a smooth outcome of the probability distribution n_i. The regularizer is the square norm of the first or a higher order derivative of the distribution function n_i itself, multiplied by a regularization strength parameter λ which determines the influence of this regularization term. The result is a

mean squared deviation ξ^2 that is low when a smooth distribution is obtained because then the derivatives of this function are small. We prefer not to smoothen the outcome in this way. We opt for another type of inversion method, without regularization, as applied by Strawbridge and Hallett [23] to the analysis of static light scattering measurements. We adopt this method here to treat data of magnetization measurements.

The range of allowed magnetic dipole moments is delimited by a minimum μ_{min} and a maximum μ_{max}. Alternatively, one could select a size range r_i and calculate the elements $T_{j,i}$ of the data transfer matrix $\overleftrightarrow{\mathbf{T}}$ with the radius rather than the magnetic dipole moment as the basis. The range is divided into N discrete parts each represented by a center value μ_i. Although a linear spacing would be possible, in this work the bins are spaced according to a geometrical series:

$$\mu_i = \mu_{min}[(\mu_{max}/\mu_{min})^{1/(N-1)}]^{i-1} \tag{6}$$

This distribution favors the narrow bins, at small dipole moments, rather than the wider bins, at larger dipole moments. Each bin has a similar weight in the inversion method, but the weight is proportional to the bin width when contributing to the magnetization curve. Our approach is recommended because the particles contribute to the measured magnetization with a weight factor proportional to their dipole moment and therefore the magnetization curve is dominated by the larger particles.

The essence of the non-regularization method used here is to split the range of N intervals into S subdomains, each with index s and elements n_s:

$$\mathbf{n}_s = (\mu_s, \mu_{S+s}, \mu_{2S+s} \cdots \mu_{(k-1)S+s}, \ldots)^T$$
$$k = 1, \ldots, \frac{N}{S}; \quad s = 1, \ldots, S; \quad \frac{N}{S} \in Integer \tag{7}$$

For each subdomain $\mathbf{n}_s$ Eq. (4) is solved by minimizing the mean squared deviation ξ^2 using Eq. (5). The vector representing the measured magnetic moment $\mathbf{M}_{exp}$ is unaltered, but an adapted version of the data transfer matrix $\overleftrightarrow{\mathbf{T}}_s$ with dimension $J \times N/S$ is used based on subdomain $\mathbf{n}_s$. Finally the subdomain distributions are merged into the total probability distribution $\mathbf{n}_{psd}$. The division of the complete basis vector into S equivalent subsets has two advantages [25]. First it reduces the number of dipole moments taken into account for the minimization of Eq. (5) and thereby renders the problem less ill-conditioned. Secondly, each of the subsets gives an equally probable solution of the problem; therefore, small peaks that occur only in one or a few of the subsets can be considered to originate from experimental noise.

To ensure that a solution is obtained that has physical meaning, the constraint is used that each n_i in Eq. (5) must be positive. For this purpose a non-negative least mean squares method is used, developed by Lawson and Hanson [26] and implemented in Mathematica [29]. An additional benefit of the non-negative constraint is that Eq. (4) is less ill-conditioned.

A large number N of different discrete magnetic dipole moment values gives a high resolution in the magnetic dipole moment (or size) but can give rise to noisy peaks in the probability distribution. With this solution one can reconstruct a precise magnetization curve. This is the optimal choice for a monomodal system with low polydispersity or a multimodal system with small ratios of the magnetic dipole moment or size. With a small number N of intervals, a smooth probability distribution is obtained, with the disadvantage of peak broadening or failure to distinguish peaks in case of a multimodal system. The latter is comparable to a high regularization parameter λ in regularization methods. The mean squared deviation ξ^2 is increased in case of a small number of intervals, meaning a lower quality of the fit of the magnetization curve. For a system with a broad distribution, a small number of intervals can be acceptable. The number of subdomains S has an optimum related to the number of intervals N. A too small or too large number of subdomains do not eliminate the ill-condition of the inversion problem.

The first bins of the histogram, representing small magnetic dipole moments (or particle sizes) often contain noise. To arrive at an objective cutoff value that discriminates between the noise and the 'real' part of the signal, we utilize the fact that smaller magnetic moments require a higher magnetic field H to reach magnetic saturation of the sample. The available experimental equipment determines the maximum magnetic field that can be reached; this fixes the minimum magnetic moment that can be measured (for details, see Supporting Information). Values below this threshold are rejected for the evaluation of the quality of the recovered test distribution in the simulations where a superparamagnetic magnetization curve is generated.

Our procedure is implemented in the computer program MINORIM, made available for several platforms [30].

3. Experimental methods

The magnetic particles used to demonstrate the inversion method are magnetite nanoparticles synthesized by single-step thermal decomposition of iron oleate. The followed chemical recipe is from the Hyeon group [31] and was described as the "sphere synthesis" by Luigjes et al. [10]. Two batches of particles were prepared containing magnetite particles with a diameter of 6.4 ± 0.6 nm and 10.5 ± 1.2 nm, respectively. The surface of the particles was coated with oleic acid, and the particles were dispersed in the solvent cis/trans-decalin (Merck, for synthesis).

Transmission electron microscopy on these samples was performed using a FEI Tecnai 12 electron microscope operated at 120 keV. For each sample, the size distribution was obtained by measuring the diameter of 200–300 particles with the iTEM software package.

For the preparation of the magnetic samples, the saturation magnetization of the two nanoparticle dispersions was measured first. Two stock dispersions were then prepared with approximately equal magnetic moment per unit volume. Finally, from these stock solutions, mixtures were prepared with well defined amounts of large and small particles.

The magnetization curves were measured with alternating gradient magnetometry (AGM) using a Princeton Micromag Model 2900. The absence of magnetic interactions between the particles was verified by comparing the shape of the normalized magnetization curve before and after dilution by a factor of 10. In the absence of dipole–dipole interactions, both normalized curves should be equal.

The first step in the analysis of the magnetization curves was the correction for non-superparamagnetic behavior. The high-field part of the curve is independent of the distribution of the dipole moments and only depends on the average dipole moment; the superparamagnetic component of the magnetization curve could thus be separated from the linear diamagnetic component by fitting it with a hyperbolic function. The magnetization curve now corrected for linear contributions was used as input for the inversion routine, which returns the experimental particle size distribution $\mathbf{n}_{psd,exp}$. A detailed overview of the complete analysis procedure is presented in the Supporting Information. For the conversion from magnetic dipole moment to magnetic radius, we assume that the magnetic objects are spherical particles with a volume magnetization equal to the bulk magnetization of 480 kA/m [32].

Numerical simulations were performed to test the limits of our inversion method. The basis vector for this simulated distribution was chosen geometrically with approximately 10 times more

points per decade than used in the inversion method, to mimic a continuous distribution. The number distribution vector **n** was filled with a mono- or bi-modal distribution for which the bin content was log-normally distributed, with known average dipole moment and standard deviation. This distribution was inserted in Eq. (4), yielding the simulated magnetization curve, $\mathbf{M}_{sim}$, with a base vector **H** containing the same values for the magnetic field strength as the experimental data. Finally, Gaussian noise was added to the magnetization curve with standard deviations from 0.001% to 1% of the saturation magnetization, typical for experiments (see next section). This simulated magnetization curve was used as input for the inversion routine to obtain the simulated size distribution $\mathbf{n}_{psd,sim}$.

4. Results and discussion

The applicability of our inversion method is tested both with experimental data and numerical simulations. The first part of this section presents the analysis of a mixture of small (6.4 nm) and large (10.5 nm) nanoparticles mixed in different ratios. The second part explores the practical limits of the inversion method using numerically simulated data.

4.1. Experiments

Fig. 2 compares the number distribution of magnetic sizes obtained with the inversion method and the particles sizes from TEM. Both distributions contain two distinct peaks, corresponding to the large and small particles mixed to obtain the magnetic sample. For both peaks, the magnetic radius (R_M) is smaller than the physical particle size (R_P). This is a well-known effect [11] due to the weaker magnetism of a near-surface layer of the nanoparticles. In our case, the difference between the magnetic radius and TEM radius is about 1 nm for both the small and large particles, consistent with a surface effect.

The most common method to analyze the magnetization curves of ferrofluids is a fit assuming a log-normal distribution. Fig. 3 compares that fit method with our inversion method for the same sample. The inversion method shows a residual that is centered around zero, evidenced by the residuals and the histogram of the deviations in the inset of Fig. 3A. The autocorrelation of these residuals (data not shown) showed the absence of any correlation, indicating that the residuals are randomly distributed around zero; this confirms that the quality of the fit is good. The log-normal distribution is not able to describe the system properly, as is clearly visible by repetitive deviations from zero in the residual (Fig. 3B). The noise level on this magnetization curve is typical for experimental data; the histogram in Fig. 3A indicates that the noise is Gaussian, with a standard deviation on the order of 1% of the saturation magnetization.

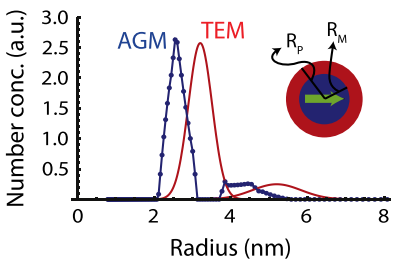

Fig. 2. Particle size distribution from magnetic measurements (AGM, line with dots) and TEM (line without dots). The inset shows a schematic picture of a magnetic nanoparticle with a magnetic core and a more weakly magnetized shell, resulting in a discrepancy between the magnetic (R_M) and TEM (R_P) radii.

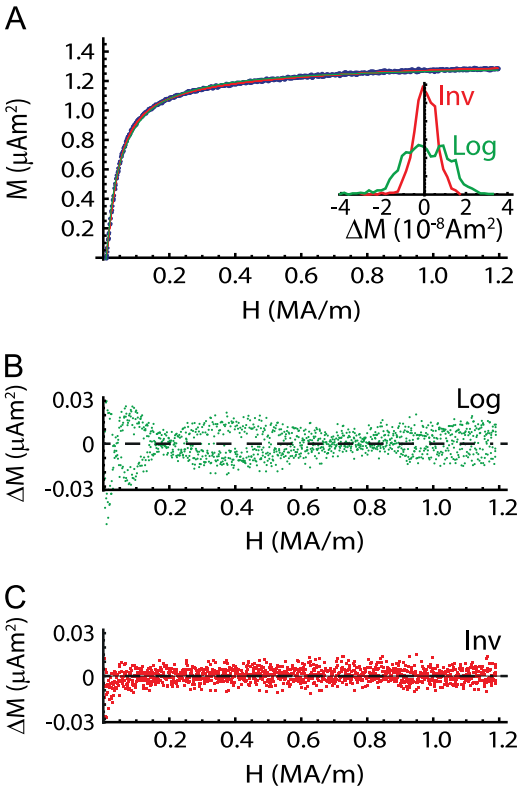

Fig. 3. (A) Experimental magnetization curve fitted using a log-normal model (Log) and the inversion method described in this work (Inv). (B) Residuals of the log-normal fit, and (C) residuals of the inversion method. The inset in (A) shows the histogram of the residuals. Close-ups of (A) are presented in the Supporting Information.

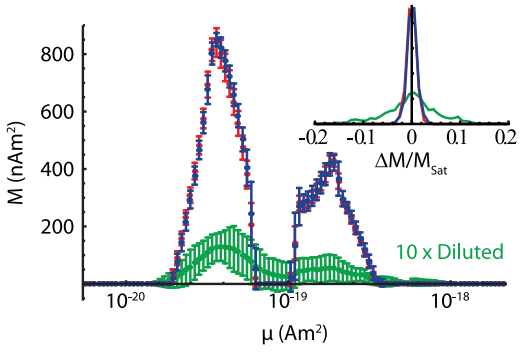

Fig. 4. Dipole moment distributions averaged over 10 different measurements on two duplicate samples containing small and large particles with a magnetization ratio of 1.97. Both samples yield indistinguishable distributions with a ratio of the peak areas of 1.96. The third sample had the same total volume but was diluted by a factor of 10; this leads to a poor signal-to-noise ratio ($\Delta M/M_{sat}$, see inset) but still to a similar distribution. In the Supporting Information, a normalized version of this figure is shown to compare the different peak ratios.

To obtain statistics on the reliability of the results, we performed 10 measurements on 3 different samples containing small and large particles; two samples were duplicates and the third one was diluted by a factor of 10. In Fig. 4, the averaged magnetic particle size distributions are shown. The error bars indicate the standard deviation for each bin. As expected, all curves show two separate peaks, even the low concentration sample, for which the standard deviation of the noise is 10% of the saturation magnetization. The two samples with the same high concentrations yield practically indistinguishable results, which confirms the reproducibility of the inversion method.

An important criterion to judge the applicability of the inversion method is whether the peaks in the resulting dipole moment distribution have the expected physical meaning. We tested this requirement by creating mixtures with different amounts of the two monodisperse stock dispersions and by measuring the magnetization curve. From the results of the analysis of the magnetization curves with the inversion method, the volumetric fractions of small particles were calculated; they are shown in Fig. 5 as a function of the weighed-in volume fraction of small particles in the mixture. The solid line has a slope of unity, indicating that the relative amounts of small and large particles were determined correctly from the magnetic analysis.

4.2. Simulations

The main variables that influence the quality of the final fit are noise (see Fig. 4), the range of sampling points of the magnetization curve, and the number N of sampling dipole moments. In this section, the influence of these parameters on the final result is investigated using simulated magnetization curves. The agreement between the simulated dipole moment distribution and that obtained from the inversion method is quantified using the R^2 value, defined as

$$R^2 = 1 - \frac{\sum_\mu \left(\mathbf{n}_{Exp}(\mu) - \mathbf{n}_{Sim}(\mu)\right)^2}{\sum_\mu \left(\mathbf{n}_{Exp}(\mu) - \langle \mathbf{n}_{Exp}(\mu)\rangle\right)^2} \tag{8}$$

where $\mathbf{n}$ is the dipole moment distribution function from the simulated (sim, sampled at μ_{exp}) and analyzed (exp) dataset. The summation runs over all values of μ present in the fitted distribution.

The Langevin curve at low field strength and high field strength only depends on, respectively, the average squared dipole moment and the average dipole moment (see Supporting Information). We therefore examined what the boundaries are of the useful region that does contain the information about the magnetic distribution; these can be found by analyzing the minimal and maximal field strengths for which a good fit is acquired with the inversion method. In Fig. 6A, the fit quality is calculated for field strengths from 0 to α (disks) and from α to 6 (squares), where α is the dimensionless magnetic field strength (see Eq. (1)). In order for the inversion method to yield dipole moments in agreement with the initially simulated distribution, all information about the distribution must be present in the analyzed part of the magnetization curve. The upper bound of this range is found by analysing magnetization curves with increasing maximum field strength until the R^2 value comes close to 1, which is found for $\alpha > 3$. The lower limit is obtained similarly by varying the lowest magnetic field value until R^2 deviates from 1, which happens for $\alpha > 2$. From these two boundaries it becomes clear that all information about the size distribution is located between $\alpha \sim 2$ and $\alpha \sim 3$ and a good quality of the measurement in this region is required.

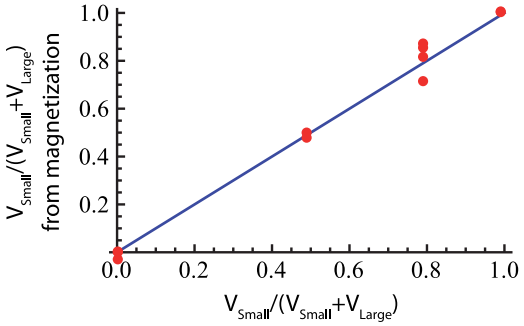

Fig. 5. Ratio of the volume of small particles dispersion (V_{Small}) to the total sample volume ($V_{Small}+V_{Large}$) obtained from the analysis of magnetic measurements with the inversion method plotted as a function of the weighed-in volume ratio of the two components in the sample. The solid line has a slope of unity.

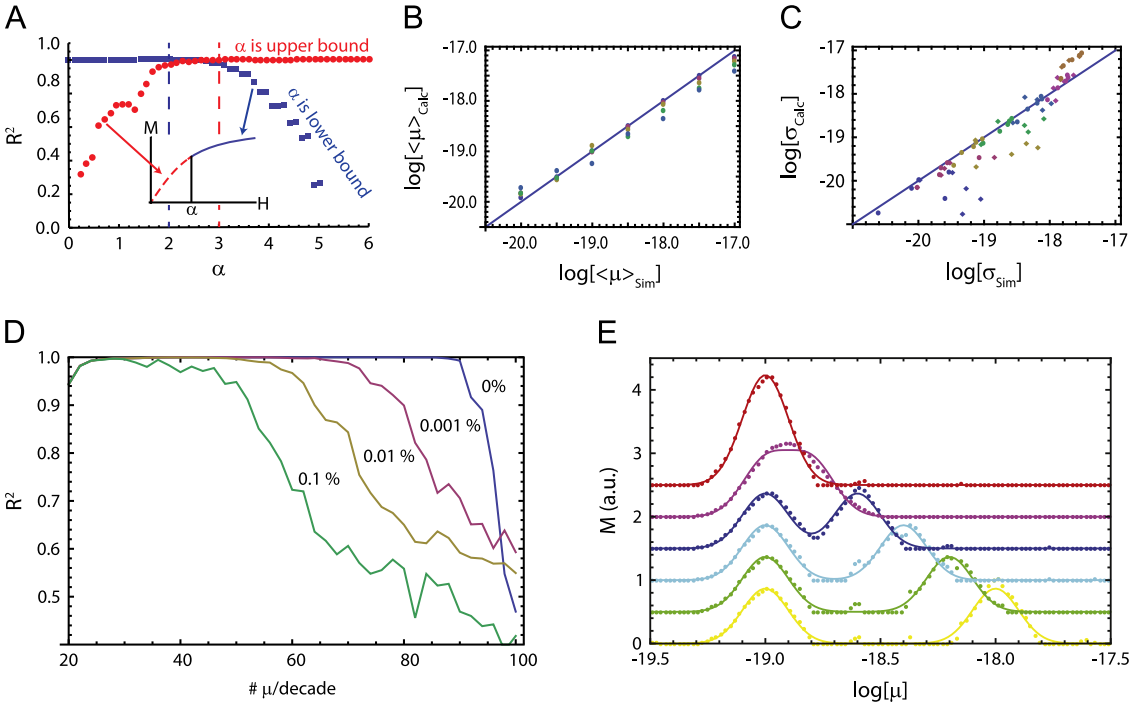

Fig. 6. (A) Fit quality expressed in a R^2 parameter (see Eq. (8)) for dimensionless magnetic field strengths from 0 to α (disks) and from α to $\alpha = 10$ (squares). The region where both ranges yield a reasonable fit contains most information about the distribution shape. (B) Calculated average dipole moment plotted against the simulated average dipole moment and (C) calculated and simulated standard deviations of a simulation with 0.01% noise (circles) and 1% noise (diamonds). In both cases the agreement is good. (D) Correlation coefficient plotted as a function of the number of dipole moment values per decade used for the calculated distribution. With increasing noise, the agreement at high number of dipole moments per decade decreases. The same happens at a low number of dipole moments per decade due to insufficient resolution to resolve the sharp peaks. (E) Comparison of the simulated (solid line) and calculated (dots) distribution for a bimodal system with different dipole moments.

In Fig. 6B and C, the average and the standard deviation of reconstructed dipole moment distributions are compared with the distributions used to calculate the magnetization curves. In both graphs the solid line has a slope of unity, indicating agreement between simulation and calculation. Fig. 6B shows the average dipole moment of a sample with 1% Gaussian noise, more noise than in most experiments; the agreement between simulated and fitted average dipole moment is still good. The same holds for the standard deviation. Although the scatter is much stronger if the sample has a high noise level, in both cases the results follow the 'best fit' line well. This good agreement indicates that, although the noise might be too high to obtain a reliable distribution, the integrated results are still physically meaningful.

Fig. 6D shows the fit quality, expressed as R^2, as a function of the number of bins per decade of the histogram used to reconstruct the distribution. At low resolution, the peaks are broadened and therefore the fit quality is lowered. The fit quality also decreases if the number of dipole moments per decade becomes too high. The onset of this decrease depends on the noise, but for typical experimental systems, this is always above 40 dipole moment values per decade.

The final test for this analysis method is its capability to separate two distinct distributions. In Fig. 6E, an example is shown with different dipole moment ratios, with a noise standard deviation of 0.1%. In this example, the calculated dipole moment distributions are in good agreement with the theoretical distribution, but this strongly depends on both the noise and number of dipole moment values per decade.

5. Conclusion

In this work, we have demonstrated an inversion method previously used to analyze light scattering data and now applied to the analysis of magnetization curves. With this method, the magnetic size distribution of ferrofluids can be resolved independently of an a priori assumed shape of the distribution. Both with experimental data and numerical simulations, the resulting distribution is in good agreement with the known distribution of particle sizes or dipole moments in the test system. Using this method it is possible to obtain the distribution shape of particle sizes or dipole moments from AGM, VSM, or other measurement techniques that yield the magnetization curves of magnetic fluids.

Appendix A. Supplementary material

Supplementary data associated with this article can be found in the online version at http://dx.doi.org/10.1016/j.jmmm.2013.10.025.

References

[1] Q.A. Pankhurst, J. Connolly, S.K. Jones, J. Dobson, Applications of magnetic nanoparticles in biomedicine, J. Phys. D: Appl. Phys. 36 (13) (2003) R167–R181.
[2] K.M. Krishnan, Biomedical nanomagnetics: a spin through possibilities in imaging, diagnostics, and therapy, IEEE Trans. Magn. 46 (7) (2010) 2523–2558.
[3] B. Gleich, J. Weizenecker, Tomographic imaging using the nonlinear response of magnetic particles, Nature 435 (2005) 1214.
[4] M. Klokkenburg, C. Vonk, E.M. Claesson, J.D. Meeldijk, B.H. Erné, A.P. Philipse, Direct imaging of zero-field dipolar structures in colloidal dispersions of synthetic magnetite, J. Am. Chem. Soc. 126 (2004) 16706.
[5] R.E. Rosensweig, Heating magnetic fluid with alternating magnetic field, J. Magn. Magn. Mater. 252 (2002) 370.
[6] R.W. Chantrell, J. Popplewell, Stuart.W. Charles, Measurements of particle size distribution parameters in ferrofluids, IEEE Trans. Magn. 14 (5) (1978) 975–977.
[7] M. Rasa, Magnetic properties and magneto-birefringence of magnetic fluids, Eur. Phys. J. E 2 (3) (2000) 265–275.
[8] A. Ivanov, S. Kantorovich, E. Reznikov, C. Holm, A. Pshenichnikov, A. Lebedev, A. Chremos, P.J. Camp, Magnetic properties of polydisperse ferrofluids: a critical comparison between experiment, theory, and computer simulation, Phys. Rev. E 75 (6) (2007) 1–12.
[9] J.C. Bacri, R. Perzynski, D. Salin, V. Cabuil, R. Massart, Magnetic colloidal properties of ionic ferrofluids, J. Magn. Magn. Mater. 62 (1) (1986) 36–46.
[10] B. Luigjes, S.M.C. Woudenberg, R. De Groot, J.D. Meeldijk, H.M. Torres Galvis, K.P. De Jong, A.P. Philipse, B.H. Erné, Diverging geometric and magnetic size distributions of iron oxide nanocrystals, J. Phys. Chem. C 115 (30) (2011) 14598–14605.
[11] D.X. Chen, A. Sanchez, E. Taboada, A. Roig, N. Sun, H.C. Gu, Size determination of superparamagnetic nanoparticles from magnetization curve, J. Appl. Phys. 105 (8) (2009) 083924.
[12] W. Brown, Dynamic Light Scattering: The Method and Some Applications, Clarendon Press, Oxford, 1993.
[13] A. Kákay, M.W. Gutowski, L. Takacs, V. Franco, L.K. Varga, Langevin granulometry of the particle size distribution, J. Phys. A: Math. Gen. 37 (23) (2004) 6027–6041.
[14] G. Lei, K.R. Shao, Y.B. Li, G.Y. Yang, Y. Guo, J. Zhu, J.D. Lavers, Bayesian inversion method and its information determination for the estimation of particle size distribution in ferrofluids, IEEE Trans. Magn. 45 (10) (2009) 3981–3984.
[15] T. Weser, K. Stierstadt, Discrete particle-size distribution in ferrofluids, Zeit. Phys. B-Condens. Matter 59 (3) (1985) 253–256.
[16] D.V. Berkov, P. Görnert, N. Buske, C. Gansau, J. Mueller, M. Giersig, W. Neumann, D. Su, New method for the determination of the particle magnetic moment distribution in a ferrofluid, J. Phys. D: Appl. Phys. 33 (2000) 331.
[17] J.A. Potton, G.J. Daniell, A.D. Eastop, M. Kitching, D. Melville, S. Poslad, B.D. Rainford, H. Stanley, Ferrofluid particle-size distributions from magnetization and small-angle neutron-scattering data, J. Magn. Magn. Mater. 39 (1–2) (1983) 95–98.
[18] J. Skilling and S. Sibisi, Maximum entropy and Bayesian methods, in: Proceedings of the Fourteenth International Workshop on Maximum Entropy and Bayesian Methods, Cambridge, England, 1994; Kluwer Academic Publishers, Dordrecht; Boston, 1996. ID: 34990181.
[19] W.H. Press, S.A. Teukolsky, W.T. Vetterling, B.P. Flannery, Numerical Recipes: The Art of Scientific Computing, Cambridge University Press, 2007.
[20] V. John, I. Angelov, A.A. Öncül, D. Thévenin, Techniques for the reconstruction of a distribution from a finite number of its moments, Chem. Eng. Sci. 62 (11) (2007) 2890–2904.
[21] S.W. Provencher, A constrained regularization method for inverting data represented be linear algebraic or integral-equations, Comput. Phys. Commun. 27 (3) (1982) 213–227.
[22] S.W. Provencher, CONTIN - a general-purpose constrained regularization program for inverting noisy linear algebraic and integral-equations, Comput. Phys. Commun. 27 (3) (1982) 229–242.
[23] K.B. Strawbridge, F.R. Hallett, Size distributions obtained from the inversion of I(q) using integrated light-scattering spectroscopy, Macromolecules 27 (8) (1994) 2283–2290.
[24] E.R. Pike, D. Watson, F.M. Watson, Measurement of Suspended Particles by Quasi-Elastic Light Scattering, John Wiley and Sons, New York, 1983.
[25] I.D. Morrison, E.F. Grabowski, C.A. Herb, Improved techniques for particle-size determination by quasi-elastic light-scattering, Langmuir 1 (4) (1985) 496–501.
[26] C.L. Lawson, R.J. Hanson, Solving Least Squares Problems, Prentice-Hall, Englewood Cliffs, 1974.
[27] A.N. Tikhonov, Solution of incorrectly formulated problems and regularization method, Sov. Math. 4 (1963) 1035–1038.
[28] A.N. Tikhonov, A. Goncharsky, V.V. Stepanov, A.G. Yagola, Numerical Methods for the Solution of Ill Posed Problems, Kluwer, Dordrecht, 1995.
[29] M.D. Woodhams, M.D. Hendy, Reconstructing phylogeny by quadratically approximated maximum likelihood, Bioinformatics 20 (2004) 348–354.
[30] ⟨http://hdl.handle.net/10411/10164⟩.
[31] J. Park, K. An, Y. Hwang, J.-G. Park, H.-J. Noh, J.-Y. Kim, J.-H. Park, N.-M. Hwang, T. Hyeon, Ultra-large-scale syntheses of monodisperse nanocrystals, Nat. Mater. 3 (2004) 891.
[32] S. Chikazumi, Physics of Magnetism, Wiley, New York, 1964.

Supplemental Information: Non-Regularized Inversion Method from Light Scattering Applied to Ferrofluid Magnetization Curves for Nanoparticle Size Distribution Analysis

Jos van Rijssel, Bonny W.M. Kuipers, and Ben H. Erné

October 2, 2013

S1 Outline of the algorithm

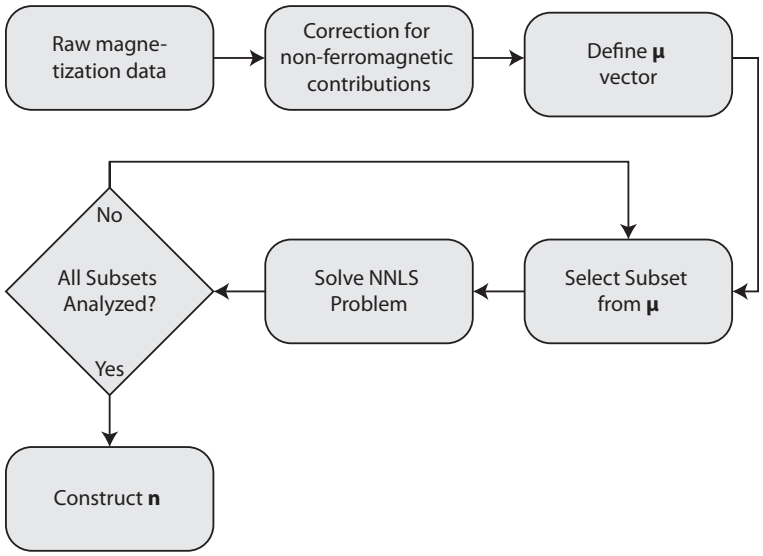

Figure S1: A flowchart of the implementation of the analysis method presented in this paper. Starting with the raw M-H data obtained from the measurements, the first step is correction for all non-ferromagnetic effects like diamagnetic signals. The mathematical foundation of this procedure is described in section S3. In the next step the base vector of the dipole moment distribution is constructed using a geometric distribution of dipole moments within a specified minimum and maximum dipole moment. The number of points is defined as the number of subsets times the number of dipole moments per subset. For each subset the reconstruction is performed by minimizing χ^2 using a NNLS algorithm developed by Lawson and Hanson[1]. If the reconstruction is complete for all subsets, the final distribution histogram is constructed from the subset histograms, and this final distribution is saved to disk.

S2 High and low field approximations

The magnetic moment of a ferrofluid of (magnetically-)polydisperse noninteracting spherical nanoparticles can be described as:

$$M(H) = N \int \mu P(\mu) L(\mu, H) \mathrm{d}\mu + \chi_{dia} H \tag{1}$$

Here we will determine the shape of $M(H)$ in the low field limit (i.e. $\alpha \to 0$) and the high field limit (i.e. $\alpha \to \infty$) were we use the dimensionless magnetic field strength α defined as:

$$\alpha = \frac{\mu_0 \mu H}{k_B T} \tag{2}$$

S2.1 Low Field limit

The Langevin equation in the low field limit simplifies to:

$$L(\alpha) = \frac{\alpha}{3} = \frac{\mu_0 \mu H}{3 k_B T} \tag{3}$$

Inserting this into Equation 1 we obtain:

$$M(H) = N \int (\mu P(\mu) \alpha / 3) \mathrm{d}\mu + \chi_{dia} H \tag{4}$$

which simplifies to:

$$M(H) = N \frac{\mu_0 H}{3 k_B T} \int \mu^2 P(\mu) \mathrm{d}\mu + \chi_{dia} H \tag{5}$$

$$= N \frac{\mu_0 H}{3 k_B T} \langle \mu^2 \rangle + \chi_{dia} H \tag{6}$$

S2.2 High Field limit

For $\alpha \to \infty$, the term $coth(\alpha) = 1$ and by plugging in the definition of α we obtain:

$$M(H) = N \int \mu P(\mu) \underbrace{\coth(\alpha)}_{=1} \mathrm{d}\mu - N \int \mu P(\mu) \frac{1}{\alpha} \mathrm{d}\mu + \chi_{dia} H \tag{7}$$

$$= N \int \mu P(\mu) \mathrm{d}\mu - N \frac{k_B T}{\mu_0 H} \int P(\mu) \mathrm{d}\mu + \chi_{dia} H \tag{8}$$

$$= N \langle \mu \rangle - N \frac{k_B T}{\mu_0 H} + \chi_{dia} H \tag{9}$$

$$= N \langle \mu \rangle \left(1 - \frac{k_B T}{\mu_0 \langle \mu \rangle H} \right) + \chi_{dia} H \tag{10}$$

$$= M_s \left(1 - \frac{k_B T}{\mu_0 \langle \mu \rangle H} \right) + \chi_{dia} H \tag{11}$$

where $M_s = N \langle \mu \rangle$

In conclusion, it is shown that in the limits of high and low field, the magnetization curve is independent of the shape of the distribution, i.e., the integral can be solved analytically, and these limits can therefore be used to correct the distribution from non-Langevin contributions.

S3 Diamagnetic correction

Before the analysis of the experimental magnetization curves obtained with AGM, in most cases, a correction for the diamagnetic contribution has to be applied. This correction is especially important for the outcome of the analysis in the small dipole regime. In this section the method for this correction is described and its influence on the detection of small dipoles is discussed. The full experimental magnetization curve, M(H), can be described as:

$$M(H) = N \int \mu P(\mu) L(\mu, H) d\mu + \chi_{dia} H \tag{12}$$

where N is the total number of particles in the sample, $P(\mu)$ the number fraction of particles with a dipole moment μ, $L(\mu, H)$ the Langevin function, χ_{dia} the diamagnetic contribution and H the magnetic field strength. In section S2 we derived an equation for the high field part of the magnetization curve:

$$M(H) = M_s \left(1 - \frac{k_B T}{\mu_0 \langle \mu \rangle H}\right) + \chi_{dia} H \tag{13}$$

where $\langle \mu \rangle$ is the average dipole moment of the sample. By fitting this to the high field region of the magnetization curve, the saturation magnetization, the diamagnetic contribution, and the average dipole moment can be obtained. The magnetic field region where this method can be applied depends on the smallest dipole moment present. Or the other way around, the choice of the high field boundary determines the lowest possible value for μ that can be obtained. The approximation of the Langevin function is valid if α is larger than 3 (see figure S2). By combining this condition with Equation 2 we obtain at room temperature:

$$\mu H > 0.98 \times 10^{-14} \mathrm{A}^2\,\mathrm{m} \tag{14}$$

This means that for a typical high field range of $H \geq 10^6$A/m, the minimal dipole moment which can be measured is: $\sim 1 \times 10^{-20}\mathrm{Am}^2$. However, the choice of this boundary does not influence the minimal dipole moment too much. Even if this boundary is 5×10^5 A/m (more than half of our experimental field range) the minimal dipole moment increases with a factor of 2. This implies also that most of the information is present in a small portion of the data (see discussion of figure 6A in the main text).

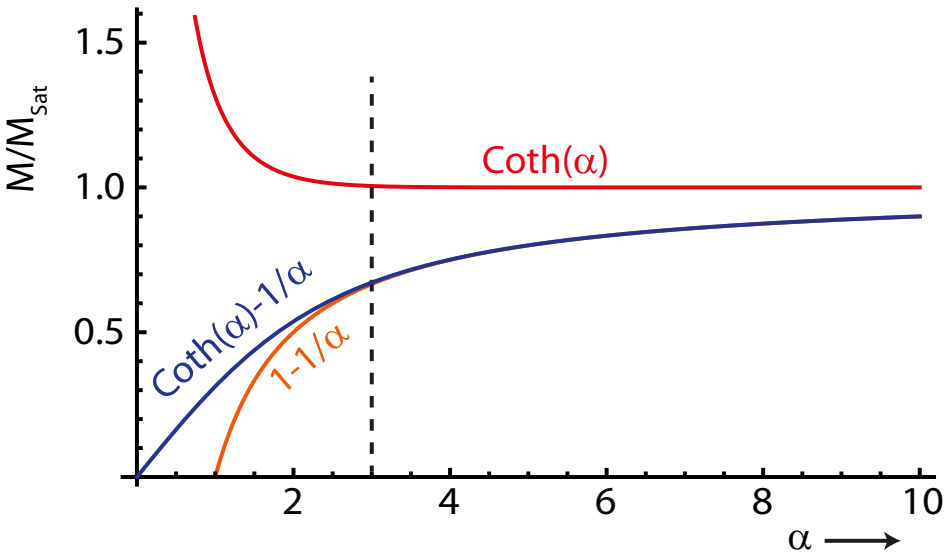

Figure S2: The Langevin equation (blue) and approximations. Above $\alpha = 3$, the hyperbolic cotangent part (red) is approximately 1 and the Langevin equation can be described by the hyperbolic part (yellow) only.

S4 Comparison of the results of a log-normal fit and the inversion method

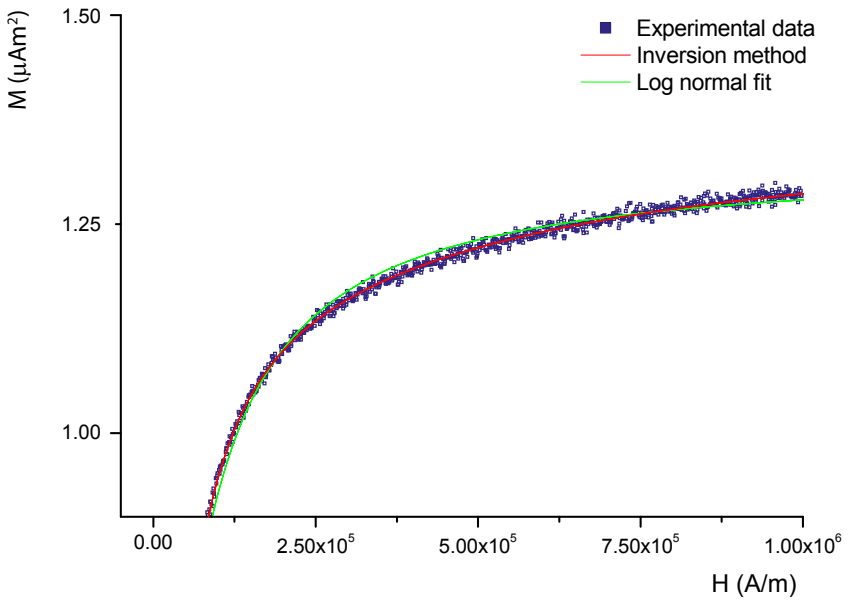

Figure S3: Close-up of the most highly curved region which contains most of the information of the magnetic size distribution. The blue dots are the experimental data (blue) and the results of the inversion method (red) and the log-normal fitting method (green) are indicated by the solid lines.

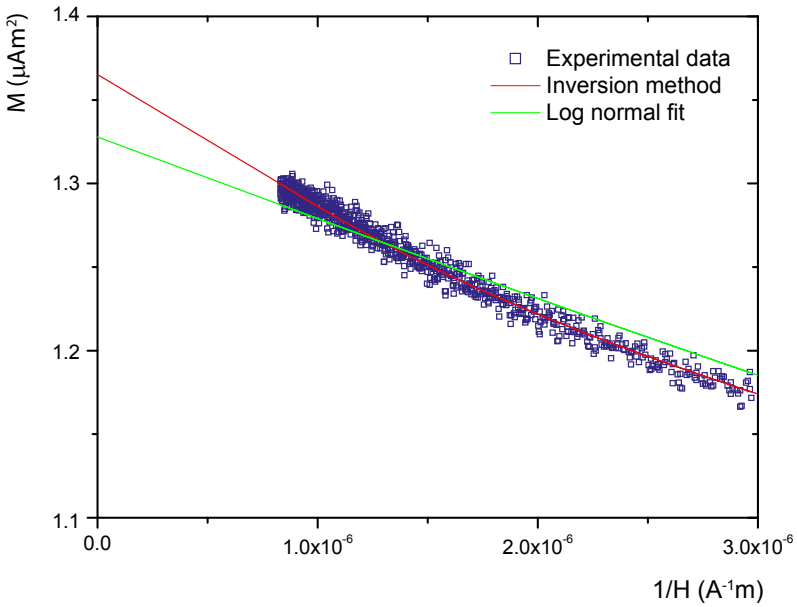

Figure S4: A plot of the magnetic moment as function of the inverse magnetic field from which the saturation magnetization can be determined from an extrapolation to zero. The difference in apparent saturation magnetization between the raw data (blue squares) and the inversion method (red line) when compared to the log-normal fit (green line) is evident.

S5 Averaged Dipole moment distributions

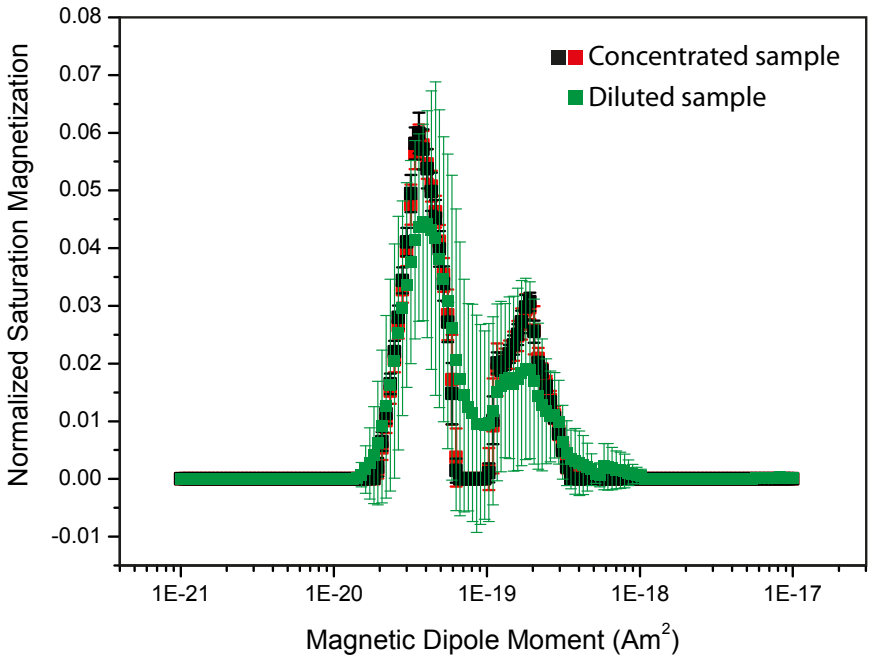

Figure S5: Dipole moment distributions normalized to the total saturation magnetization. The red and black points are from a similar sample while the green curve has a ten times lower nanoparticle concentration.

References

[1] C. L. Lawson and R. J. Hanson. *Solving least squares problems.* Prentice-Hall, Englewood Cliffs, 1974.